Journal of Computational Physics 233 (2013) 227–240

Contents lists available at SciVerse ScienceDirect

Journal of Computational Physics

journal homepage: www.elsevier.com/locate/jcp

A Fully Eulerian formulation for fluid–structure-interaction problems

Thomas Richter *

Institute for Applied Mathematics, University of Heidelberg, INF 294, 69120 Heidelberg, Germany

ARTICLE INFO

Article history:
Received 25 February 2012
Received in revised form 15 August 2012
Accepted 24 August 2012
Available online 13 September 2012

Keywords:
Finite elements
Fluid–structure interaction
Eulerian
Monolithic
Interface-capturing

ABSTRACT

In this work, we present a Fully Eulerian framework for fluid–structure interaction (fsi) problems coupling the incompressible Navier–Stokes equations with a hyperelastic solid.

The Fully Eulerian framework is a monolithic implicit variational formulation for the coupled problem. In contrast to the well-established Arbitrary Lagrangian Eulerian (ALE) coordinates, the Fully Eulerian framework formulates both subproblems, fluid and solid, in Eulerian coordinates. This concept circumvents various difficulties connected to ALE coordinates since no artificial domain mapping is used. The formulation is an interface-capturing method and uses an extension of the solid's deformation, the *Initial Point Set*, to detect the interface location.

By construction, very large deformation as well as topology changes like contact of the solid to the domain boundary or other solid parts are possible.

1. Introduction

We present a monolithic variational finite element method for fluid–structure interaction problems. Emphasis is on applications where very large structural deformations, free movement of the structure within a flow domain and contact of the structure with the domain's boundary, with other structures or self-contact appears. The formulation presented in this work is Eulerian–Eulerian and a first variant of this novel approach has been suggested by Dunne [14,15].

There exist countless different approaches to model and simulate fluid–structure interaction problems. Among them, we focus on monolithic models, where the complete problem is formulated in one coupled system including the interface conditions between solid and fluid. Monolithic models allow for implicit solution schemes, large timesteps and offer the possibility to use sensitivity based error estimation and optimization methods. They are well suited for the simulation of problems with large fluid densities as appearing in hemodynamics [18]. While fluid problems are naturally described in a fixed Eulerian coordinate framework, a Lagrangian, material centered description is the usual basis for solid problems. All monolithic schemes for a fluid–solid interaction must somehow match these two different frameworks.

In Lagrangian or arbitrary Lagrangian methods, the flow problem is mapped onto a matching reference domain. Classical approaches are the ALE method, see [29,4,35] or deforming-spatial-domain/ stabilized space–time methods (DSD/SST), see for instance [53,51]. These formulations have in common, that kinematic and dynamic coupling conditions are easily embedded into trial spaces and established by variational techniques. A drawback of Lagrangian methods is the underlying transformation of the fluid-problem which can break down for large deformations or large solid movements. Lagrangian approaches are interface-tracking methods as the common interface is shared by both subproblems.

The Eulerian–Lagrangian methods use a Eulerian fixed computational mesh for the fluid problem and a Lagrangian mesh for the solid problems. Coupling of the two frameworks is accomplished by using force densities as in the immersed boundary method by Peskin [43] or the immersed interface method [39]. Other approaches introduce additional interface variables

* Tel.: +49 6221 54 5448.
E-mail address: thomas.richter@iwr.uni-heidelberg.de

0021-9991/$ - see front matter © 2012 Elsevier Inc. All rights reserved.
http://dx.doi.org/10.1016/j.jcp.2012.08.047

and couple the two systems using Lagrange multipliers. Examples are the fictitious domain method [22], or other recent approaches based on the extended finite element method [20]. A survey of interface coupling approaches is given by Felippa et. al. [17]. Eulerian–Lagrangian methods are interface-capturing approaches. The interface is not part of the fixed Eulerian fluid mesh and its location within the computational fluid domain must be captured implicitely as part of the solution scheme. An early approach for capturing the interface is the Volume of Fluid method [30], where a tracking function Φ_V takes the value one in the fluid domain and zero in the solid domain. This function Φ_V is transported with the interface velocity. A proper numerical approximation of Φ_V with a sharp jump from fluid to solid domain is one of the difficulties connected to this scheme. Another possibility for capturing the interface – at first used to model multiphase-flows – is by means of a scalar Level-Set [42,47] function Φ_L which in any point of the domain indicates the signed distance to the interface. The interface itself is given as zero-contour of the Level-Set function. Based on Level-Sets, very efficient and simple numerical schemes exist to describe free-boundary and fluid–structure interactions [38]. Usually, Level-Set representations of the interface lack the ability to reproduce sharp corners. A general problem of Eulerian–Lagrangian methods are the approximation properties close to the interface. Since the fluid elements are cut by the interface and the solution may be discontinuous (or at least not differentiable) across the interface, approximation with standard finite elements is difficult. Here, the extended finite element method helps to improve accuracy [11,20].

Finally, for problems with very large deformation, an Eulerian description of the structural problem is desirable [54,41]. Using a fixed Eulerian background mesh, the interface between fluid and solid will freely move in the domain. A Eulerian method will always be of interface-capturing type. Dunne [14] and Dunne et al. [15] has first implementations of an Eulerian-Eulerian model for the interaction of an incompressible fluid with an hyper-elastic solid. Here, capturing of the interface is accomplished with the Initial Point Set (IPS), a vector-field Φ_{IPS} used to transport the complete reference coordinate system. The IPS-method is able to capture interfaces with sharp edges. A finite difference approach for Eulerian–Eulerian fluid–structure interaction based on the Volume of Fluid method [30] is introduced by Sugiyama et al. [50]. Here, the coupling between incompressible fluid and structure is solved with a pressure correction iteration. An Eulerian-Eulerian fluid–structure interaction method based on Level-Set functions is introduced by He and Qiao [23]. Four Level-Set functions are required to represent the moving structure domain. Two of them take a role similar to the Initial Point Set as introduced by Dunne [14] and Dunne et al. [15].

The Fully Eulerian formulation introduced in this work is based on extensions of the IPS method [46,16,44]. Fluid and solid problem are given in an Eulerian formulation, the interface conditions are embedded in the function spaces and realized by variational load balancing. For capturing the interface the solid's deformation will be extended to only a small layer in the fluid domain. The flow problem is modeled without any transformation and apart from the small interface layer no additional variables must be introduced, making the method very efficient.

In the second section we shortly introduce the required notation. Section 3 is devoted to the governing equations in Eulerian coordinates and deals with the coupling of fluid and solid problem. Details on discretization and the solution scheme are provided in Section 4. Finally, in Section 5 we present different numerical examples demonstrating the scope of this new Fully Eulerian fluid–structure interaction formulation. We conclude in Section 6.

2. Preliminaries

Let $\Omega \subset \mathbb{R}^2$ be a two dimensional domain. At time $t = 0$ this domain is split into a non-overlapping partitioning into the fluid part $\hat{\Omega}_f := \Omega_f(0)$ and solid part $\hat{\Omega}_s := \Omega_s(0)$ with a common interface $\hat{\Gamma}_i := \partial\hat{\Omega}_f \cap \partial\hat{\Omega}_s$. We will consider problems, where the domain partitioning will change in time, the combined domain Ω however will be fixed:

$$\hat{\Omega}_f \mapsto \Omega_f(t), \quad \hat{\Omega}_s \mapsto \Omega_s(t), \quad \Gamma_i(t) = \partial\Omega_f(t) \cap \partial\Omega_s(t), \quad \Omega = \Omega_f(t) \cup \Omega_s(t).$$

At time $t = 0$ we call $\hat{\Omega}_f$ and $\hat{\Omega}_s$ the reference configuration. In the context of fluid–structure interaction, $\hat{\Omega}_s$ refers to the Lagrangian view-point and $\Omega_s(t)$ to the Eulerian. For simplicity, we will consider problems with Dirichlet boundary conditions only and define

$$\Gamma_f(t) := \partial\Omega_f(t) \cap \partial\Omega, \quad \Gamma_s(t) := \partial\Omega_s(t) \cap \partial\Omega.$$

As function spaces we use the Lebesgue space $L^2(\Omega)$ in the domain Ω or in the (moving) subdomains as well as Sobolev-spaces $H^m(\Omega)$ of L^2 functions with weak derivatives in L^2. By $(\cdot,\cdot)_\Omega$ we denote the L^2-inner product and by $\|\cdot\|_\Omega$ the usual L^2-norm on Ω. Further, by $\langle\cdot,\cdot\rangle_\Gamma$ we denote the L^2-inner product on (parts of) the boundary $\Gamma \subset \partial\Omega$, usually the inner interface between the two subdomains. By $H^1(\Omega)$ we denote the Lebesgue space of L^2-functions with first weak derivative in L^2 and by $H^1_0(\Omega;\Gamma)$ the space of H^1-functions with trace zero on (parts of) the boundary $\Gamma \subset \partial\Omega$.

3. Eulerian formulation of fluid structure interaction

In this section we derive the coupled system of equations describing the interaction of an incompressible Stokes or Navier–Stokes fluid with an elastic structure of St. Venant Kirchhoff type. All equations are given in variational formulation. This allows for an easy transformation between Eulerian and Lagrangian coordinate frameworks.

3.1. Eulerian description of fluid flows

Fluid problems are naturally given in the Eulerian coordinate framework. Here, the flow domain $\Omega_f(t)$ is moving in time along with the interface $\Gamma_i(t)$ to the solid domain. On this interface, a no-slip condition is assumed for the viscous fluid. Let $v_i(t)$ be an extension of the interface-velocity into the fluid domain. Then, velocity and pressure are given as

$$\begin{aligned} &v_f(t) \in v_i(t) + \mathcal{V}_f(t), \quad p_f(t) \in \mathcal{L}_f(t) : \rho_f(\partial_t v_f(t) + v_f(t)\cdot\nabla v_f(t), \phi_f)_{\Omega_f(t)} + (\sigma_f(t), \nabla\phi_f)_{\Omega_f(t)} \\ &\quad = \rho_f(f_f(t), \phi_f)_{\Omega_f(t)} (\operatorname{div} v_f(t), \xi_f)_{\Omega_f(t)} = 0 \quad \forall \phi_f \in \mathcal{V}_f(t),\ \forall \xi_f \in \mathcal{L}_f(t), \end{aligned} \tag{1}$$

where by $\mathcal{V}_f(t)$ and $\mathcal{L}_f(t)$ we denote suitable H^1-function spaces for velocity and L^2-spaces for the pressure on the moving domain $\Omega_f(t)$. The Cauchy-stress tensor is given by

$$\sigma_f := \rho_f \nu_f \left(\nabla v_f + \nabla v_f^T\right) - p_f I,$$

where by ρ_f we denote the fluid's density and by ν_f its kinematic viscosity.

3.2. Lagrangian description of a St. Venant Kirchhoff material

In natural Lagrangian coordinates, elastic structures are modeled by describing the deformation of the reference domain $\hat{\Omega}_s := \Omega_s(0)$ via $\hat{T}_s(t) := \mathrm{id} + \hat{u}_s(t) : \hat{\Omega}_s \to \Omega_s(t)$. The computational domain $\hat{\Omega}_s$ is fixed. On $\hat{\Gamma}_i := \Gamma_i(0)$ we drive the problem by interface-stresses coming from the flow domain. Let $\hat{F}_s := I + \hat{\nabla}\hat{u}_s$ be the deformation gradient, $\hat{J}_s := \det \hat{F}_s$ its determinant and $\hat{v}_s := d_t\hat{u}_s$ the solid's velocity. The hyperelastic material is governed by:

$$\begin{aligned} &\hat{u}_s(t) \in \hat{\mathcal{V}}_s, \quad \hat{v}_s(t) \in \hat{\mathcal{L}}_s : (\hat{\rho}_s d_t\hat{v}_s(t), \hat{\phi}_s)_{\hat{\Omega}_s} + (\hat{F}_s(t)\hat{\Sigma}_s(t), \hat{\nabla}\hat{\phi}_s)_{\hat{\Omega}_s} = \hat{\rho}_s(\hat{f}_s(t), \hat{\phi}_s)_{\hat{\Omega}_s} + \langle \hat{g}_s(t), \hat{\phi}\rangle_{\hat{\Gamma}_i}(d_t\hat{u}_s(t), \hat{\psi}_s)_{\hat{\Omega}_s} \\ &\quad = (\hat{v}_s(t), \hat{\psi}_s)_{\hat{\Omega}_s} \quad \forall \hat{\phi}_s \in \hat{\mathcal{V}}_s,\ \forall \hat{\psi}_s \in \hat{\mathcal{L}}_s. \end{aligned} \tag{2}$$

Again, by $\hat{\mathcal{V}}_s$ and $\hat{\mathcal{L}}_s$ we denote suitable function spaces on $\hat{\Omega}_s$. By $\hat{g}_s$ we denote interface-stresses on the interface boundary and by $\hat{\rho}_s$ the solid's density (in unloaded reference configuration). With the Lamé coefficient λ_s and shear modulus μ_s the second Piola Kirchhoff stress tensor for a St. Venant Kirchhoff material [31] is given by

$$\hat{\Sigma}_s := 2\mu_s\hat{E}_s + \lambda_s \mathrm{tr}(\hat{E}_s) I, \tag{3}$$

where $\hat{E}_s := \frac{1}{2}(\hat{F}_s^T\hat{F}_s - I)$ is the Green–Lagrange strain tensor.

3.3. Eulerian description of a St. Venant Kirchhoff material

The Eulerian version of solid Eq. (2) is derived by simple integral transformation using the natural mapping to the Eulerian framework $\hat{T}_s(t) : \hat{\Omega}_s \mapsto \Omega_s(t)$. First, for an Eulerian coordinate $x := \hat{x} + \hat{u}_s(\hat{x}, t)$ we define on $\Omega_s(t)$ the Eulerian deformation $u_s(t) \in \mathcal{V}_s(t)$ and velocity $v_s(t) \in \mathcal{L}_s(t)$:

$$u_s(x,t) := \hat{u}_s(\hat{x}, t), \quad v_s(x,t) := \hat{v}_s(\hat{x}, t).$$

These definitions allow us to introduce an inverse mapping $T_s(t) : \Omega_s(t) \to \hat{\Omega}_s$ back to the reference domain, its deformation gradient F_s and determinant J_s:

$$T_s(x,t) := x - u_s(x,t), \quad F_s := \nabla T_s = I - \nabla u_s, \quad J_s := \det F_s. \tag{4}$$

With the relation $T_s(t) \circ \hat{T}_s(t) = \mathrm{id}$, it follows in Eulerian coordinates:

$$F_s\hat{F}_s = I \quad \Rightarrow \quad F_s = \hat{F}_s^{-1}, \quad J_s := \hat{J}_s^{-1}, \quad E_s := \frac{1}{2}(F_s^{-T}F_s^{-1} - I). \tag{5}$$

Next, let $\hat{\phi}(t) \in \hat{\mathcal{V}}_s$ be arbitrary with Eulerian counterpart $\phi(t) \in \mathcal{V}_s(t)$ defined by $\phi(x) := \hat{\phi}(\hat{x})$. Then, it holds:

$$\hat{\nabla}\hat{\phi} = \nabla\phi F_s^{-1}, \quad d_t\phi = \partial_t\phi + v_s\cdot\nabla\phi. \tag{6}$$

Integral transformation of (2) using (4)–(6) gives the Eulerian formulation of the solid problem:

$$\begin{aligned} &u_s(t) \in \mathcal{V}_s(t), \quad v_s(t) \in \mathcal{L}_s(t) : (\hat{\rho}_s J_s(\partial_t v_s + v_s\cdot\nabla v_s), \phi_s)_{\Omega_s(t)} + (\sigma_s, \nabla\phi_s)_{\Omega_s(t)} \\ &\quad = (J_s\hat{\rho}_s f_s, \phi_s)_{\Omega_s(t)} + \langle g_s, \phi_s\rangle_{\Gamma_i(t)} (J_s(\partial_t u_s + v_s\cdot\nabla u_s), \psi_s)_{\Omega_s(t)} = (J_s v_s, \psi_s)_{\Omega_s(t)} \quad \forall \phi_s \in \mathcal{V}_s(t),\ \forall \psi_s \in \mathcal{L}_s(t), \end{aligned} \tag{7}$$

where the Cauchy stress tensor in Eulerian formulation reads:

$$\sigma_s = J_s F_s^{-1}\Sigma_s F_s^{-T} = J_s F_s^{-1}\left(2\mu_s E_s + \lambda_s \mathrm{tr}(E_s)\right)F_s^{-T}, \quad E_s := \frac{1}{2}(F^{-T}F^{-1} - I).$$

In Eulerian framework, the solid's density gets $\rho_s(x,t) = J_s(x,t)\hat{\rho}_s(\hat{x})$. Transition to Eulerian coordinates gives rise to convective terms in the momentum equation as well as the velocity-deformation relation. These terms have to be carefully resolved by the discretization scheme. We give details in Section 4.2.

3.4. Coupled fluid structure interaction problem in Eulerian coordinates

Coupling of (1) and (7) is accomplished by prescribing balancing conditions for velocity and normal stresses on the common interface:

$$v_f(t) = v_s(t), \quad \sigma_f(t)n(t) = \sigma_s(t)n(t) \quad \text{on} \quad \Gamma_i(t). \tag{8}$$

We realize these conditions by variational techniques. Continuity of velocities is incorporated in one globally defined and "continuous" trial space $\mathcal{V}$ on $\Omega = \Omega_f(t) \cup \Omega_s(t)$. For $v(t) \in \mathcal{V}$ we use the notation $v_f(t) := v_{|\Omega_f(t)}$ and $v_s(t) := v_{|\Omega_s(t)}$. While looking straightforward, prescribing continuity of the velocities reveals a regularity problem that is discussed in literature [13]: without further damping, the structure's velocity lacks the required regularity to have a well-defined trace on $\Gamma_i(t)$. Although being fundamental, we do not elaborate on this issue here.

The dynamic condition coupling the normal-stresses is realized by means of variationally consistent load evaluation [10,21] choosing common and "continuous" test-functions $\phi \in \mathcal{V}$ with $\phi_s := \phi_{|\Omega_s(t)}$ and $\phi_f := \phi_{|\Omega_f(t)}$. Then, the dynamic condition is inherently given ($g_s = 0$) with integration by parts. It holds for the relevant terms in the momentum equation:

$$(\sigma_f, \nabla\phi_f)_{\Omega_f} + (\sigma_s, \nabla\phi_s)_{\Omega_s} = -(\operatorname{div}\sigma_f, \phi_f)_{\Omega_f} - (\operatorname{div}\sigma_s, \phi_s)_{\Omega_s} + \int_{\partial\Omega_f} \sigma_f n_f \cdot \phi_f \mathrm{d}o + \int_{\partial\Omega_s} \sigma_s n_s \cdot \phi_s \mathrm{d}o,$$

where by n_f and n_s we denote the outward facing normal vectors at the subdomains boundary. On boundaries with Dirichlet condition, these boundary integrals vanish due to $\phi = 0$. On the common interface Γ_i, it holds $n_f = -n_s$. Further, with $\phi := \phi_f = \phi_s$ on Γ_i we get

$$\int_{\Gamma_i} \sigma_f n_f \cdot \phi_f \mathrm{d}o + \int_{\Gamma_i} \sigma_s n_s \cdot \phi_s \mathrm{d}o = \int_{\Gamma_i} (\sigma_f - \sigma_s) n \cdot \phi \,\mathrm{d}o,$$

where we have picked $n := n_f$. Therefore, continuity of stresses $\sigma_f n = \sigma_s n$ holds by variational principles. For simplicity of notation we introduce characteristic functions with respect to the two subdomains:

$$\chi_f(x,t) := \begin{cases} 1 & x \in \Omega_f(t) \\ 0 & x \in \Omega_s(t) \end{cases}, \quad \chi_s(x,t) := \begin{cases} 1 & x \in \Omega_s(t) \\ 0 & x \in \Omega_f(t) \end{cases}. \tag{9}$$

Combining (1) and (7) the coupled fsi problem is given using the globally defined function spaces:

$$\begin{aligned} &v \in \mathcal{V}, \quad u_s \in \mathcal{V}_s, \quad p_f \in \mathcal{L}_f : \Big((\rho_f\chi_f + J_s\rho_s\chi_s)(\partial_t v + v \cdot \nabla v), \phi\Big) + \Big(\sigma_f\chi_f + \sigma_s\chi_s, \nabla\phi\Big) \\ &\quad = \Big(\rho_f f_f \chi_f + J_s \rho_s f_s \chi_s, \phi\Big) (\operatorname{div} v_f, \xi_f)_{\Omega_f(t)} = 0 (J_s(\partial_t u_s + v \cdot \nabla u_s), \psi_s)_{\Omega_s(t)} = (J_s v_s, \psi_s)_{\Omega_s(t)} \quad \forall \phi \in \mathcal{V},\ \xi_f \in \mathcal{L}_f \quad \psi_s \in \mathcal{L}_s. \end{aligned} \tag{10}$$

The crux of this very simple looking variational formulation is the partitioning of the domain Ω into the two subdomains described by (9). The characteristic functions depend on the solution, namely on u_s, itself. Dunne et al. [15] used the deformation to introduce an additional global vector field, the *Initial Point Set* Φ_{IPS} which at time $t = 0$ is the identity $\Phi(x,0) = x$ and then transported with the solid's velocity v_s and its extension to the fluid-domain. This IPS function helps to find a reference location of every Eulerian point. We further simplify this approach by directly using the Eulerian inverse transformation $T_s(t) := \mathrm{id} - u_s(t) : \Omega_s(t) \to \hat{\Omega}_s$ and its extension to define the characteristic functions:

$$\chi_s(x,t) := \begin{cases} 1 & x - u(x,t) \in \hat{\Omega}_s \\ 0 & x - u(x,t) \notin \hat{\Omega}_s \end{cases}, \quad \chi_f(x,t) := 1 - \chi_s(x,t), \tag{11}$$

where $u : \Omega \to \mathbb{R}^2$ is an extension of u_s to the whole domain. The extension u of the solid's deformation u_s establishes the *Initial Point Set* by the relation $\Phi_{\text{IPS}}(x,t) := x - u_s(x,t)$. Note, that for a fluid-coordinate $x \in \Omega_f(t)$ we do not necessarily require $x - u_s(x,t) \in \hat{\Omega}_f$, see (11).

3.5. Comparison to ALE formulations

In the classical ALE formulation for FSI problems the structure problem is formulated on the static reference domain $\hat{\Omega}_s$ and the flow problem is mapped onto the fixed matching domain $\hat{\Omega}_f$ via $\hat{T}_f(\hat{x},t) := \hat{x} + \hat{u}_f(\hat{x},t)$, where $\hat{u}_f = \text{ext}_f(\hat{u}_s)$ is an extension of the solid's deformation field to the flow domain, see [35,36,21,2]. By this transformation, the interface does not move in the computational domain and can easily be resolved with high accuracy. As a drawback, strong nonlinearities are introduced. For comparison with (10), the variational formulation of the coupled ALE system is given by:

$$\begin{aligned} &(\hat{J}\rho_f \partial_t \hat{v}_f + \rho_f \hat{F}^{-1}(\hat{v}_f - \partial_t \hat{T}_f) \cdot \hat{\nabla} \hat{v}_f, \hat{\phi})_{\hat{\Omega}_f} + (\hat{J}\hat{\sigma}_f \hat{F}^{-T}, \hat{\nabla}\hat{\phi})_{\hat{\Omega}_f} + (\hat{\rho}_s \partial_t \hat{v}_s, \hat{\phi})_{\hat{\Omega}_s} + (\hat{F}\hat{\Sigma}_s, \hat{\nabla}\hat{\phi})_{\hat{\Omega}_s} \\ &\quad = (\hat{J}\rho_f \hat{f}_f, \hat{\phi})_{\hat{\Omega}_f} + (\rho_s \hat{f}_s, \hat{\phi})_{\hat{\Omega}_s} (\widehat{\operatorname{div}}(\hat{J}\hat{F}^{-1}\hat{v}_f), \hat{\xi})_{\hat{\Omega}_f} + (d_t \hat{u}_s - \hat{v}_s, \hat{\psi})_{\hat{\Omega}_s} = 0, \end{aligned}$$

with deformation gradient $\hat{F} := I + \hat{\nabla}\hat{u}$, its determinant $\hat{J}$ and the stress tensors in Lagrangian formulation:

$$\hat{\sigma}_f := \rho_f \nu_f (\hat{\nabla} v_f \hat{F}^{-1} + \hat{F}^{-T} \hat{\nabla} \hat{v}_f^T) - \hat{p} I, \quad \hat{\Sigma}_s := \mu_s \hat{E}_s + \lambda_s \mathrm{tr}(\hat{E}_s).$$

In both formulations, Eulerian and ALE, an extension of the deformation into the fluid domain is introduced. The conceptual difference between the Eulerian and ALE formulation is the use of the deformation-extension to the flow domain. In ALE, this extension is used to establish a mapping $\hat{T}_f(\hat{\Omega}_f) = \Omega_f(t)$ for the transformation of the equations. This gives rise to one fundamental problem: if the mapping gets irregular, i.e. $\hat{J}_f := \det(\hat{\nabla}\hat{T}_f) \to 0/\infty$, the ALE formulation will break down. This is unavoidable in the case of very large movement (e.g. permanent rotation of a free solid) or topology change (e.g. contact of the solid with the domain's boundary).

In the Fully Eulerian formulation, the extension u_f is only used to capture the interface as a look-up function in the definition of (11). Here $T_f(\Omega_f(t)) \neq \hat{\Omega}_f$ is allowed. We only expect $T_f(\Omega_f(t)) \cap \hat{\Omega}_s = \emptyset$. This gives more freedom in the choice of the extension's boundary values. Possible regularity problems of u_f do not influence the overall scheme. For the numerical application it will turn out, that the extension u_f is only required in a small layer around $\Gamma_i(t)$. Beyond this layer it is sufficient to solve the Navier–Stokes equations without further variables. This leads to a very efficient scheme.

One major drawback of transforming the structure system to Eulerian coordinates is the introduction of convection terms in the equations. Here loss of conservation principles due to numerical diffusion has to be expected. Further, even if the coupled Eulerian system (10) does not include strong nonlinearities at first glance (like it is the case for ALE), implicit domain affiliation leads to nonlinearities in the coupling. This even holds true, if linear models (Stokes and linear elasticity) are coupled. Finally, by having the interface cut through mesh elements, a discretization will require finer meshes to get accuracies similar to those of the ALE approach.

4. Discretization

In this section, we describe the discretization scheme used to approximate the fluid–structure interaction system (10). In short, we use a semi-implicit time stepping scheme for temporal discretization and a stabilized equal order finite element discretization in space.

4.1. Temporal discretization

Let $0 = t_0 < t_1 < \cdots < t_M = T$ be a subdivision of the time interval $[0,T]$ with (possibly non uniform) step-size $k_m := t_m - t_{m-1}$. By $u_k = (u_s^m)_{m=0}^M$, $v_k = (v^m)_{m=0}^M$ and $p_k = (p_f^m)_{m=0}^M$ we define the solution $U^m := \{v^m, u_s^m, p_f^m\}$ at the discrete time-step t_m. Every time-step is split into two sub-steps: (1) we march in time $U^{m-1} \to \tilde{U}^m$ using the old domain-partitioning at time t_{m-1}. (2) we update the domain partitioning $\Gamma_i^{m-1} \to \Gamma_i^m$ by extending the new solid-deformation $\tilde{u}_s^m$ and then project the solution to the new domains $\tilde{U}^m \to U^m$.

(1) *time-marching* For simplicity, we define $\chi_{f/s}^m := \chi(t_m)_{f/s}$, $\Omega_{f/s}^m := \Omega_{f/s}(t_m)$, and combine trial-spaces and test-spaces to

$$U^m \in \mathcal{X}^m := \mathcal{V} \times \mathcal{V}_s(t_m) \times \mathcal{L}_f(t_m), \quad \Phi \in \mathcal{Y}^m := \mathcal{V} \times \mathcal{L}_s(t_m) \times \mathcal{L}_f(t_m).$$

For time-stepping, we use the θ-scheme and starting with $U^{m-1} \in \mathcal{X}^{m-1}$ we find the intermediate $\tilde{U}^m \in \mathcal{X}^{m-1}$ by

$$\tilde{U}^m \in \mathcal{X}^{m-1} : A^{m-1}(\tilde{U}^m)(\Phi) = 0 \quad \forall \Phi \in \mathcal{Y}^{m-1}, \tag{12}$$

with the test-functions $\Phi := \{\phi, \psi_s, \xi_f\} \in \mathcal{Y}^{m-1}$ and the semilinear form

$$\begin{aligned}
A^{m-1}(\tilde{U}^m)(\Phi) = {} & k_m^{-1} \Big((\rho_f \chi_f^{m-1} + \tilde{J}_s^m \rho_s \chi_s^{m-1})(\tilde{v}^m - v^{m-1}, \phi) \Big)_\Omega + (\mathrm{div}\, \tilde{v}^m, \xi_f)_{\Omega_f^{m-1}} \\
& + \Big(\rho_f (\theta \tilde{v}^m \cdot \nabla \tilde{v}^m + (1-\theta) v^{m-1} \cdot \nabla v^{m-1}), \phi \Big)_{\Omega_f^{m-1}} \\
& + \Big(\rho_s (\theta \tilde{J}_s^m \tilde{v}^m \cdot \nabla \tilde{v}^m + (1-\theta) J_s^{m-1} v^{m-1} \cdot \nabla v^{m-1}), \phi \Big)_{\Omega_s^{m-1}} + \Big(\theta \tilde{\sigma}_f^m + (1-\theta)\sigma_f^{m-1}, \phi \Big)_{\Omega_f^{m-1}} \\
& + \big(\theta \tilde{\sigma}_s^m + (1-\theta)\sigma_s^{m-1}, \phi \big)_{\Omega_s^{m-1}} + k_m^{-1} \big(\tilde{u}^m - u^{m-1}, \psi_s \big)_{\Omega_s^{m-1}} \\
& + \big(\theta \tilde{v}^m \cdot \nabla \tilde{u}^m + (1-\theta) v^{m-1} \cdot \nabla u^{m-1}, \psi_s \big)_{\Omega_s^{m-1}} - \big(\theta \tilde{v}^m + (1-\theta) v^{m-1}, \psi_s \big)_{\Omega_s^{m-1}} \\
& - \rho_f (\theta f_f^m + (1-\theta) f_f^{m-1}, \phi)_{\Omega_f^{m-1}} - \rho_s (\theta \tilde{J}_s^m f_s^m + (1-\theta) J_s^{m-1} f_s^{m-1}, \phi)_{\Omega_s^{m-1}}.
\end{aligned} \tag{13}$$

The scalar parameter $\theta \in (0,1]$ controls the time-stepping scheme. For $\theta = 1$ we get a variant of the implicit Euler scheme, for $\theta = 1/2$ the well known Crank–Nicolson scheme which is of second order in the time. Since we use a first order explicit representation of the domain affiliation by freezing the characteristic functions at the old time step t_{m-1} we cannot expect second order convergence of the overall scheme in the general case. Nevertheless, we choose an implicitely shifted variant of Crank–Nicolson with $\theta = \frac{1}{2} + O(k)$ to avoid excessive numerical dissipation in the fluid equation while formally preserving second order accuracy, see [26,27,40]. The intermediate solution $\tilde{U}^m \in \mathcal{X}^{m-1}$ at time t_m is still given on the old domain partitioning belonging to t_{m-1}. Transition to $\mathcal{X}^m$ is accomplished in the second substep.

(2) *extension step*. To generate a new partition $\Gamma_i^{m-1} \to \Gamma_i^m$ we need to extend the intermediate deformation $\tilde{u}_s^m$ to the entire domain. Then, given $\tilde{u}^m : \Omega \to \mathbb{R}^2$ we can define the new domain partitioning with help of the characteristic functions (11):

$$\tilde{u}^{m-1} := \begin{cases} \tilde{u}_s^{m-1} & \text{in } \Omega_s^{m-1} \\ \text{ext}_f(\tilde{u}_s^{m-1}) & \text{in } \Omega_f^{m-1} \end{cases}, \quad \chi_s^m := \begin{cases} 1 & x - \tilde{u}^{m-1}(x,t) \in \hat{\Omega}_s \\ 0 & x - \tilde{u}^{m-1}(x,t) \notin \hat{\Omega}_s \end{cases}.$$

Projection of $\tilde{U}^{m-1}$ to the new domain partitioning is accomplished by simply restricting the extensions to the corresponding subdomains:

$$v^m := \tilde{v}^{m-1}, \quad u_s^m := \tilde{u}^{m-1}|_{\Omega_s^m}, \quad p_f^m := \tilde{p}^{m-1}|_{\Omega_f^m}.$$

This very simple extension and projection operation will limit the overall accuracy of the scheme to $O(k)$. For obtaining higher order schemes, time-stepping should be performed on space–time slabs similar to the DSD/SST formulation introduced by Tezduyar [52]. For extending the deformation one should use an extension operator which preserves the stiffness of the structure like the biharmonic operator, see [25]. However, since we will introduce a discrete extension on the algebraic level we skip further discussions at this point.

4.2. Spatial finite element discretization

Eq. (12) is discretized by a finite element method using continuous, piece-wise polynomial equal order elements. First, by Ω_h, we denote a triangulation of the domain Ω into quadrilaterals. Ω_h consists of open, non-overlapping elements $K \in \Omega_h$ and all elements have interior angles which are bound close to $\pi/2$ in order to prevent too sharp or blunt corners. Details on principals of finite element meshes as well as necessary modifications to deal with adaptive meshes and local mesh refinement are given in the literature [12,7,3]. Let $Q^{(r)} = \text{span}\{x^i y^j,\ 0 \leqslant i,j \leqslant r\}$ be the polynomial space of degree r in every direction. On Ω_h, we define by V_h the usual isoparametric finite element space of degree r:

$$V_h = \{\phi \in C(\bar{\Omega}), \quad \forall K \in \Omega_h : \phi|_K \circ T_K^{-1} \in Q^{(r)}, \quad Q^{(r)} \ni T_K : (0,1)^2 \to K\}. \tag{14}$$

This space (with the required modification at Dirichlet boundaries) is used for all solution variables. The triangulation Ω_h must not necessarily be aligned with the fluid and structure domain as it is usually the case in ALE formulations. Since the interface Γ_i is moving, an alignment would ask for mesh-motion or even remeshing in every step. Besides the effort for accomplishing a tracking mesh, such a scheme would require careful projection of the solution between the time-steps. Conservation of physical principles, in particular incompressibility is very cumbersome, see e.g. [5].

Hence, an element K can be cut by the interface $\Gamma_i(t)$ and be part of both subdomains. We introduce (overlapping) subpartitionings for the fluid-mesh, the solid-mesh and the interface-mesh:

$$\Omega_{f/s,h}^m := \{K \in \Omega_h; K \cap \Omega_{f/s}^m \neq \emptyset\}, \quad \Omega_{i,h}^m := \Omega_{f,h}^m \cap \Omega_{s,h}^m.$$

See the left sketch in Fig. 1 for this partitioning. The affiliation of an element $K \in \Omega_h$ to the sub-meshes will change in time. Close to the interface layer $\Omega_{i,h}$ we will use locally refined meshes for a higher resolution at this critical coupling region. See Fig. 2 for a snapshot of the solid's deformation $u_{s,h}$.

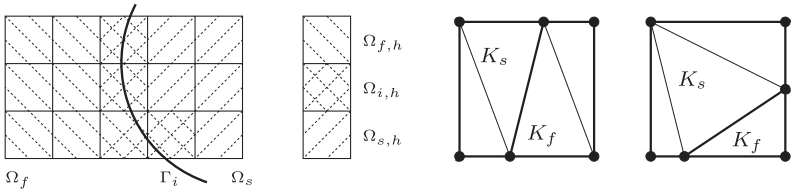

Fig. 1. Left: partitioning of a finite element triangulation into overlapping sub-meshes. Right: partitioning of interface-elements into four triangles each used for accurate numerical quadrature.

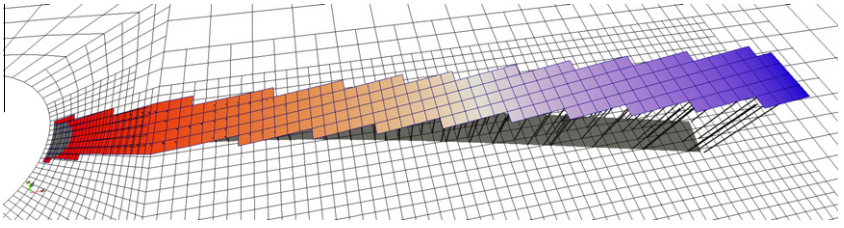

Fig. 2. Discrete deformation $u_{s,h}$ is defined only in $\Omega_{s,h}$ and on the adjacent layer of elements. The dark-shaded area denotes the real solid-domain. It is only here, that $u_{s,h}$ enters the computation.

Some of the solution variables like pressure p_f and deformation u_s are defined in parts of the domain Ω only:

$$p_{f,h} \in V^m_{f,h}, \quad u_{s,h} \in [V^m_{s,h}]^2,$$

where by $V^m_{f/s,h}$ we denote the finite element-space (14) restricted to $\Omega^m_{f,h}$ and $\Omega^m_{s,h}$, respectively. By this construction, different degrees of freedom are involved to represent a discrete function at different times. At the interface Γ_i, the discrete functions – like $p_{f,h}$ – are defined on the complete element $K \in \Omega_{i,h}$, their values however only enter the calculation within the physical domain as given by the discretized Initial Point Set. In Fig. 2, we show a plot taken from the numerical examples in Section 5 which demonstrates this construction. Here, the solid fills the dark-shaded area on the mesh. The discrete deformation $u_{s,h}$ is defined on all elements K that cover the solid-domain. This "sawtooth pattern" of the finite element solution is only used for reasons of practical implementation. The values of $u_{s,h}$ will only be used inside the solid domain $\Omega_s(t)$ given by Initial Point Set.

(1) *Spatial discretization of the time-matching step*

By $X^m_h = V_h \times V^m_{s,h} \times L^m_{f,h}$ we denote a couple of H^1-conforming isoparametric finite element space of degree $r \geqslant 1$ as described in the previous paragraph. Let $U_h := \{v_h, u_{s,h}, p_{f,h}\} \in X^m_h$ be the unknown solution and $\Phi_h := \{\phi_h, \psi_{s,h}, \xi_{f,h}\}$ the set of test-functions. Since all unknowns (velocity, deformation and pressure) are discretized with order-r-finite elements, additional stabilization terms $S(\cdot)(\cdot)$ are added to the semi-linearform $A(\cdot)(\cdot)$ (see (13)). For stabilization of the inf-sup condition as well as for convective terms arising in the momentum equation, the Local Projection Stabilization is applied, see the survey [6,45] for a first application to fluid–structure interaction problems. These stabilization terms take the form

$$S_{\mathrm{lps}}(U_h)(\Phi_h) = \sum_{K\in\Omega_h} \delta_K(v_h \cdot \nabla(v_h - \pi_h v_h), v_h \cdot \nabla(\phi_h - \pi_h \phi_h))_K + \sum_{K\in\Omega_{f,h}} \alpha_K\big(\nabla(p_{f,h} - \pi_h p_{f,h}), \nabla(p_{f,h} - \pi_h p_{f,h})\big)_K,$$

where by $\pi_h : V_h \to \tilde{V}_h$ we denote the local projection into a coarser space. Here, this coarser space is either the polynomial space with a reduced degree, or an equal-order space on a coarser mesh. See [6] for details on different choices for this local projection as well as for hints on the local choice of the stabilization parameters α_K and δ_K. The LPS method is not suitable for the second equation in (13), since it lacks any natural diffusion: (for simplicity $\theta = 1$):

$$k_m^{-1}(\tilde{u}^m - u^{m-1}, \psi_s)_{\Omega_s^{m-1}} + (\tilde{v}^m \cdot \nabla \tilde{u}^m - \tilde{v}^m, \psi_s)_{\Omega_s^{m-1}} = 0 \quad \forall \psi_s \in \mathcal{L}_s.$$

Instead, we apply the usual residual based conforming streamline diffusion method and a second stabilization term is added to the set of equations:

$$S_{\mathrm{supg}}(U_h)(\Phi_h) = \sum_{K\in\Omega_{s,h}} \Big(k_m^{-1}(\tilde{u}^m - u^{m-1} + \tilde{v}^m \cdot \nabla \tilde{u}^m - \tilde{v}^m, \gamma_K \tilde{v}^m \cdot \nabla \psi_s\Big)_{\Omega_s^{m-1}}.$$

We refer to [37] or [8] for details. The stabilized semi-linearform is denoted by $A_h(\cdot)(\cdot) := A(\cdot)(\cdot) + S_{\mathrm{lps}}(\cdot)(\cdot) + S_{\mathrm{supg}}(\cdot)(\cdot)$.

We emphasize, that deformation $u_{s,h} \in V_{s,h}$ and pressure $p_{f,h} \in L_{f,h}$ are not defined on the whole mesh. They appear only on the corresponding sub-meshes. As opposed to ALE formulation, no global extension of the solid deformation is required to solve the fluid-problem. By defining the deformation locally only on $\Omega_{s,h}$ (which is the solid domain plus the small layer of interface elements $\Omega_{i,h}$), a significant reduction of numerical effort is reached, as in many applications, the structure fills only a very small part of the entire domain. The stabilized Petrov–Galerkin-formulation of (12) reads:

$$\tilde{U}^m_h \in X^{m-1}_h : A^{m-1}_h(\tilde{U}^m_h)(\Phi_h) = 0 \quad \forall \Phi_h \in Y^{m-1}_h := V_h \times L^{m-1}_{s,h} \times L^{m-1}_{f,h}. \tag{15}$$

Since the interface $\Gamma_i(t)$ is moving through the domain and crossing mesh elements, one cannot align the mesh nodes with the interface. This is a one severe drawback compared to interface tracking formulations like ALE. Numerical integration thus has to carefully consider the interface regions that dominate the dynamics of the coupled problem. In Dunne [15] it was proposed to use summed integration formulas to evaluate integrals on elements touched by the interface. For an accurate integration a very large number of integration points is necessary. This method, not taking the specific layout of the interface into account is not efficient. Here, we approximate the interface by a piece-wise linear function and split every element touching the interface into four triangles. In the right sketch of Fig. 1 we show examples for the splitting of an element into triangles. Each triangle is integrated with a seven-point Gauss formula [49].

A further approximation problem occurs, since piece-wise polynomial finite element functions $U_h \in X_h$ are not able to correctly reflect the solution's behavior at the interface. While the velocity is continuous over Γ_i, its gradient is expected to have a jump. Here, one should use the extended finite element method [11,20] for increasing the interface accuracy.

(2) *Spatial discretization of the extension-step*

In the extension-step, we first have to extend the intermediate deformation $\tilde{u}^m_{h,s}$ into the fluid-domain. We assume, that the time-step k_m is small enough to prevent interface-movements larger than one element-size

$$k_m \|v_h\|^{-1} \leqslant h.$$

By this assumption it is sufficient to extend the deformation $\tilde{\tilde{u}}^m_h := \mathrm{ext}_h(\tilde{u}^m_{h,s})$ to at most one layer of elements into the fluid-domain. Here, we use a simple constant extension. In Fig. 3 we give a plot of a one dimensional configuration. After extending the deformation we can locate the new interface-location using the extended $\tilde{\tilde{u}}^m_h$. The new interface-location x^m_i belonging to Fig. 3 is characterized by the relation

$$x_i^m - \tilde{\tilde{u}}_h^m(x_i^m) = x_i^{m-1} - u_{h,s}^{m-1}(x_i^{m-1}).$$

Since $\tilde{\tilde{u}}_h$ is a piece-wise polynomial, this equation is easily solved for x_i^m with some few steps of a Newton's iteration. Likewise, we extend the intermediate pressure $\tilde{p}_{h,f}^m$ one layer into the solid mesh. Given the new partitioning $\Omega_{f,h}^m, \Omega_{s,h}^m$ we acquire U_h^m by restriction to the subdomains:

$$v_h^m := \tilde{v}_h^m, \quad u_{s,h}^m := \tilde{\tilde{u}}_{s,h}^m|_{\Omega_{s,h}^m}, \quad p_{f,h}^m := \tilde{\tilde{p}}_{f,h}^m|_{\Omega_{f,h}^m}.$$

4.3. Solution scheme

In every time-step $t_{m-1} \mapsto t_m$ we need to solve a large, nonlinear coupled system of discretized partial differential equations given by (13) and (15):

$$U_h \in X_h : A_h(U_h)(\Phi_h) = 0 \quad \forall \Phi_h \in Y_h,$$

where we have skipped the superscript "m" denoting the time-step. Given a suitable initial guess $U_h^{(0)}$, which is usually the old time-step $U_h^{(0)} := U_h^{m-1}$, we approximate the solution by a Newton iteration

$$W_h^{(t)} \in X_h : A_h'(U_h^{(t)})(W_h^{(t)}, \Phi_h) = -A_h(U_h^{(t)})(\Phi_h), \quad U_h^{(t+1)} := U_h^{(t)} + W_h^{(t)},$$

where by $A_h'(U_h)(W_h, \Phi_h)$ we denote the Gateaux derivative of $A_h(\cdot)(\cdot)$ in direction $W_h := \{w_h, r_h, q_h\} \in X_h$. This derivative is computed analytically based on the variational form (13). The Jacobian of the Navier–Stokes equations is standard and found in the literature. Computing the Jacobian of elastic structure equations, in particular including fluid–structure interactions is more involved, see [21,2,45] for works regarding ALE formulations. Here, due to the separate extension step, the Jacobian does not include derivatives with regard to the movement of the domain. Including these derivatives will be necessary when deriving fully implicit time-stepping schemes which will help to increase stability for larger time-steps. In this case, the derivatives with regard to the domain movement correspond to shape-derivatives as known from topology- and structure-optimization problems [48]. In the context of fluid–structure interactions or free-surface flows, these shape derivatives are analyzed by Brummelen and coworkers [58,57]. As mentioned, using the semi-implicit time-stepping scheme we only need to evaluate the derivatives with respect to the principal variables which are easily given with help of the following fundamental relations [31,45]:

$$\frac{\partial F_s^{-1}(u)}{\partial u}(\phi) = F_s^{-1}(u)\nabla\phi F_s^{-1}(u), \quad \frac{\partial J_s(u)}{\partial u}(\phi) = J_s(u)F_s^{-1}(u) : \nabla\phi.$$

For completeness, we give the full Jacobian of $A(\cdot)(\cdot)$ for the case of the backward Euler scheme ($\theta = 1$) using the notation $W := \{w, r, q\} \in X_h^{m-1}$ and skipping all indices regarding temporal and spatial discretization

$$\begin{aligned} A'(U)(W,\Phi) = {} & k_m^{-1}\Big((\rho_f\chi_f + J_s\rho_s)w + \rho_s JF^{-1} : \nabla r, \phi\Big) + (\operatorname{div} w, \xi_f)_{\Omega_f} \\ & + \Big((\rho_f\chi_f + \rho_s J\chi_s)(w\cdot\nabla v + v\cdot\nabla w) + \rho_s(JF^{-1} : \nabla r)v\cdot\nabla v, \phi\Big) + (\rho_f\nu_f(\nabla w + \nabla w^T) - qI, \nabla\phi)_{\Omega_f} \\ & + (D\sigma_s(u)(r), \nabla\phi)_{\Omega_s} + (k_m^{-1}r + v\cdot\nabla r + w\cdot\nabla u - w, \psi_s)_{\Omega_s} - (\rho_s(JF^{-1} : \nabla r), \phi)_{\Omega_s}, \end{aligned} \tag{16}$$

with the derivatives of the St. Venant Kirchhoff stress tensor in Eulerian coordinates:

$$\begin{aligned} D\sigma_s(u)(r) = {} & (F^{-1} : \nabla r)\sigma_s(u) + F^{-1}\nabla r\sigma_s(u) + \sigma_s(u)\nabla r^T F^{-T} + \mu JF^{-1}F^{-T}(\nabla r^T F^{-T} + F^{-1}\nabla r)F^{-1}F^{-T} \\ & + \lambda_s JF^{-1}\operatorname{tr}(F^{-1}\nabla r F^{-1}F^{-T})F^{-T}. \end{aligned} \tag{17}$$

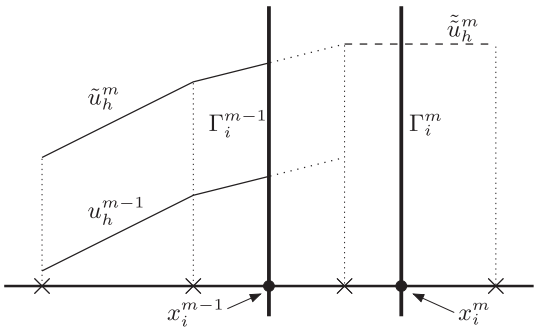

Fig. 3. Extension-step (2): old deformation u_h^{m-1} and intermediate $\tilde{u}_h^m$ (on old mesh). Extension $\tilde{\tilde{u}}_h^m$ into fluid-domain. x_i^m is new interface location.

A very efficient implementation of these derivatives is possible since most terms, like the product $F^{-1}F^{-T}$ appear very often and must be coded only once. The linear system to be solved in every step of the Newton iteration involves a very large and coupled, ill conditioned matrix given by (16) and (17). In this first work on the Eulerian method we use a direct solver for these linear problems. While multigrid methods are well established for both solid and fluid computations, the application to a coupled fluid–structure interaction problem is very involved. For efficient solving one has to exploit a partitioned structure within the multigrid smoother, see [24,32,9,19]. Application of a partitioned inner iteration to the Eulerian formulation is difficult, since the interface cuts through mesh elements and no strict partitioning is available.

5. Numerical examples

For validation of the Eulerian model, we first consider two simple fluid–structure interaction benchmarks, the *csm*-1 problem and the *fsi*-1 problem as proposed by Hron and Turek [33]. Both benchmark problems use the configuration as shown in Fig. 4, where an incompressible fluid flows around a circular obstacle and an elastic beam that is attached to this rigid obstacle. In the *csm*-1 benchmark configuration the fluid is initially at rest and the beam undergoes a deformation caused by a gravity force. In the *fsi*-1 benchmark problem no gravity force is acting, but the flow is driven by an inflow profile. Both problems have a stationary solution and highly accurate results for different functional values are available in literature [33,34]. Finally, we describe a more challenging test-case, where an elastic ball falls in an container filled with an incompressible fluid. The ball touches the bottom of the container and rebounces. Here we focus on modeling this collision of elastic structure with the domain's boundary.

5.1. Model validation: csm-1

In this first test-case, a gravity force is acting on the elastic structure $f_s := -J_s\hat{\rho}_s g_s \chi_s$ shown in Fig. 4. In the original benchmark configuration [33] $g_s = 2$ has been used, Wick [55] also published results for $g_s = 4$ yielding a larger deformation. To exploit the possibilities of very large deformation with the Eulerian approach, we add a further test-case using $g_s = 8$. We measure the deformation u_s in the tip of the beam $A = (0.6, 0.2)$ in the stationary limit. In Table 1 we present the deflections in this measurement point on different meshes with decreasing mesh sizes under three different gravity forces. For comparison, we indicate the reference values are stated in [33,34,55,56]. The complete set of parameters used in this configuration is:

$$\rho_f = \hat{\rho}_s = 10^3, \quad \nu_f = 10^{-3}, \quad \mu_s = 5 \cdot 10^5, \quad \lambda_2 = 2 \cdot 10^6, \quad f = -g_s J_s \hat{\rho}_s \chi_s \tag{18}$$

It is clearly seen, that the Full Eulerian method yields accurate values which are very close to the reference values cited from the literature. Further, the Eulerian framework is able to increase the gravity force up to a point ($g_s = 8$) where the beam touches the rigid bottom of the flow-chanel, see Fig. 5. Here, no results for comparison are available in the literature.

5.2. Model validation: fsi-1

As a second test-case of the benchmark-suite published by Hron and Turek we refer to the *fsi*-1 problem. The flow is driven by a parabolic inflow profile on the boundary Γ_{in}:

$$v_{\text{in}} = \frac{y(H-y)}{4H^2}\, v_{\max}, \quad H = 0.41, \quad v_{\max} = 0.3.$$

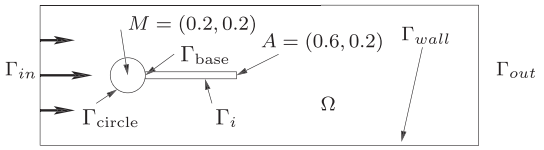

Fig. 4. Configuration of the *csm*-1 and *fsi*-1 benchmark problems as published by Hron and Turek [33].

Table 1
Results for the CSM-1 benchmark problem using increasing volume forces. Functional values on a sequence of meshes. Comparison to reference values taken from the literature using the ALE framework.

Mesh size	$g_s = 2$		$g_s = 4$		$g_s = 8$	
	$u^x(A)$	$u^y(A)$	$u^x(A)$	$u^y(A)$	$u^x(A)$	$u^y(A)$
$h_{\min} \approx 0.008$	6.372	61.84	21.22	114.54	59.846	189.74
$h_{\min} \approx 0.004$	7.116	64.70	25.02	121.25	65.760	192.03
$h_{\min} \approx 0.002$	7.149	66.07	25.10	122.16	66.857	192.35
Hron and Turek [33]	7.187	66.10	n/a	n/a	n/a	n/a
Wick [55,56]	7.150	64.90	25.33	122.30	n/a	n/a

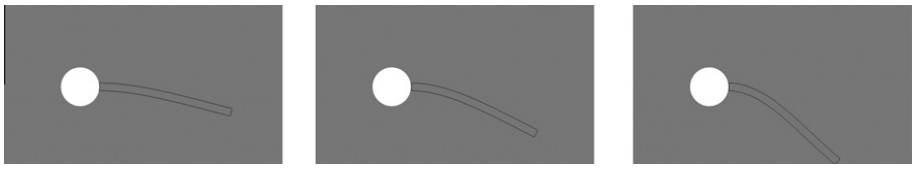

Fig. 5. Configuration of the *csm*-1 benchmark problem and modifications with larger gravity force. Left $g_s = -2$, middle $g_s = -4$ and right $g_s = -8$.

Due to a slight unbalance in the configuration (see Fig. 4) the elastic beam undergoes a small deflection. Apart from this modification, the material constants are taken as described in (18). Besides measuring the deflection of the beam, drag- and lift-values of the obstacle (rigid circle & beam) where to be estimated. Let $\Gamma_{\text{obs}} := \Gamma_i \cup \Gamma_{\text{circle}} \setminus \Gamma_{\text{base}}$ be the complete outer boundary of the obstacle. Here, we consider the drag-value:

$$J_{\text{drag}} = \int_{\Gamma_{\text{obs}}} n_f \sigma_f e_1 \, \mathrm{d}s.$$

Evaluation of these integrals is not trivial in the Eulerian setting, since Γ_{obs} depends on the solution itself and further since Γ_{obs} cuts through mesh elements which makes the integration difficult. Hence, for evaluation purposes we first modify the functionals by using the dynamic coupling condition (8) and inserting zero:

$$J_{\text{drag}} = \int_{\Gamma_{\text{circle}} \setminus \Gamma_{\text{base}}} n_f \sigma_f e_1 \, \mathrm{d}s + \int_{\Gamma_i} \underbrace{n_f \sigma_f}_{=-n_s\sigma_s} e_1 \, \mathrm{d}s \pm \int_{\Gamma_{\text{base}}} n_s \sigma_s e_1 \, \mathrm{d}s = \int_{\Gamma_{\text{circle}} \setminus \Gamma_{\text{base}}} n_f \sigma_f e_1 \, \mathrm{d}s + \int_{\Gamma_{\text{base}}} n_s \sigma_s e_1 \, \mathrm{d}s - \int_{\partial\Omega_s} n_s \sigma_s e_1 \, \mathrm{d}s.$$

In the stationary limit (and in the absence of external forces) it holds for the exact solution $\int_{\partial\Omega_s} n\sigma \, \mathrm{d}s = -\int_{\Omega_s} \mathrm{div}\sigma_s \, \mathrm{d}x = 0$ and hence:

$$J_{\text{drag}} = \int_{\Gamma_{\text{circle}}} n\sigma e_1 \, \mathrm{d}s,$$

where by n we denote the outward facing normal vector (whether in Ω_f or Ω_s) and by σ the corresponding acting tensor. Evaluation of this boundary integral is straightforward, since the boundary Γ_{circle} is fixed, even in the Eulerian setting. The accuracy of this functional evaluation can be further enhanced by expressing it in terms of variational residuals (*Babuška-Miller-Trick*) [1,10,45]. In Table 2 we gather the drag-value as obtained with the Eulerian approach. For evaluation of the functional we consider both the boundary integrals as well as the reformulation into residual terms. A good reference value $J_{\text{drag}} = 14.2940 \pm 10^{-5}$ is available in the literature [34,45]. In Fig. 6 we show the error slopes of the drag approximation. Here we observe linear order of convergence (in the mesh-size h) for the boundary integral and quadratic convergence for the

Table 2
fsi-1 Benchmark results. Drag-coefficient $J_{\text{drag}}(U_h)$ evaluates as boundary integral and reformulated as residual expression. The reference value taken from literature is given by $J_{\text{drag}} = 14.2940 \pm 10^{-5}$.

Mesh-size	Dof's	Boundary	Variational
0.1	53,450	15.1052	14.9004
0.05	176,790	15.2333	14.5971
0.025	640,490	14.7836	14.4062
0.0125	2,466,390	14.5118	14.3280

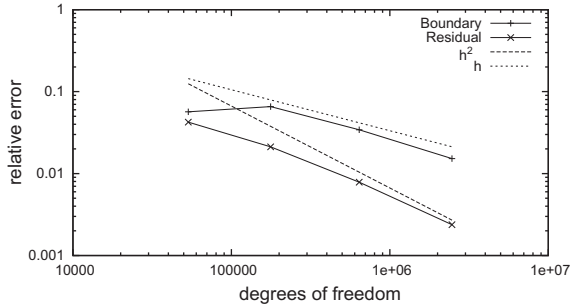

Fig. 6. Convergence of the drag-approximation with the Eulerian coordinate framework. Evaluated as boundary integral (linear convergence) and as residual term (quadratic convergence).

residual reformulation. Using piece-wise linear finite elements one would expect (at least for a pure incompressible flow problem) the double order of convergence. Here, order reduction will take place due to the limited discretization accuracy close at the elements that are cut by the moving interface. Remedy could be found by using local mesh adaptation close to the interface or considering the extended finite element method [11] for better accuracy in the interface region.

5.3. Contact problem

Finally, we model the "free fall" of an elastic ball Ω_s with radius $r_{\text{ball}} = 0.4$ in a container $\Omega = (-1,1)^2$ filled with a viscous fluid Ω_f. The container is closed at the bottom boundary $\Gamma_{\text{bot}} = \partial\Omega_{y=-1}$ but open at the top and the sides. Here, by open we refer to the "do-nothing" boundary condition

$$v\partial_n v - pn = 0,$$

which allows free in- and outflow of the fluid. See [28].

Fig. 7 shows the configuration of this test-case. At time $t = 0$, the midpoint of the ball is at $x_0 = (0,0)$. Since gravity is the only acting force on the solid, the ball will accelerate and fall to the bottom $\Gamma_{\text{bot}} = \{(x,-1),\ x \in (-1,1)\}$. At this rigid wall with homogenous Dirichlet condition $v_f = 0$, the ball stops and due to elasticity it will bounce off again. The parameters used for this test-case are given by

$$\rho_f = 10^3, \quad \hat{\rho}_s = 10^3, \quad \nu_f = 10^{-2}, \quad \mu_s = 10^4, \quad \lambda_s = 4 \cdot 10^4, \quad f = -J_s \hat{\rho}_s \chi_s.$$

As functional outputs, we measure the average y-displacement and y-velocity of the structure as well as the structure's volume:

$$j_{\text{vol}}(t) := \int_{\Omega_s(t)} 1 \, \mathrm{d}x, \quad j_u(t) := \int_{\Omega_s(t)} u_s^y(t) \, \mathrm{d}x, \quad j_v(t) := \int_{\Omega_s(t)} v_s^y(t) \, \mathrm{d}x. \tag{19}$$

In Fig. 7 we show snapshots of the solution for different times. By gravity influences, the ball is accelerated and finally touches the bottom boundary. Here, the flow comes to a rest and the ball gets compressed. Then, by its elasticity it gets stretched and bounces back.

Fig. 8 shows the progress of the functionals (19) as function over time. The left sketch shows the average deformation (which can be used to measure the position of the ball). Here it is clearly seen that due to the viscous damping of the fluid, the bounce-off height is considerably smaller than the initial height. The right sketch shows the volume of the ball. Due to the compression at impact-time, the volume gets reduced during the contact. Reduction of volume is possible, since the flow-container is open on the upper, left and right boundaries.

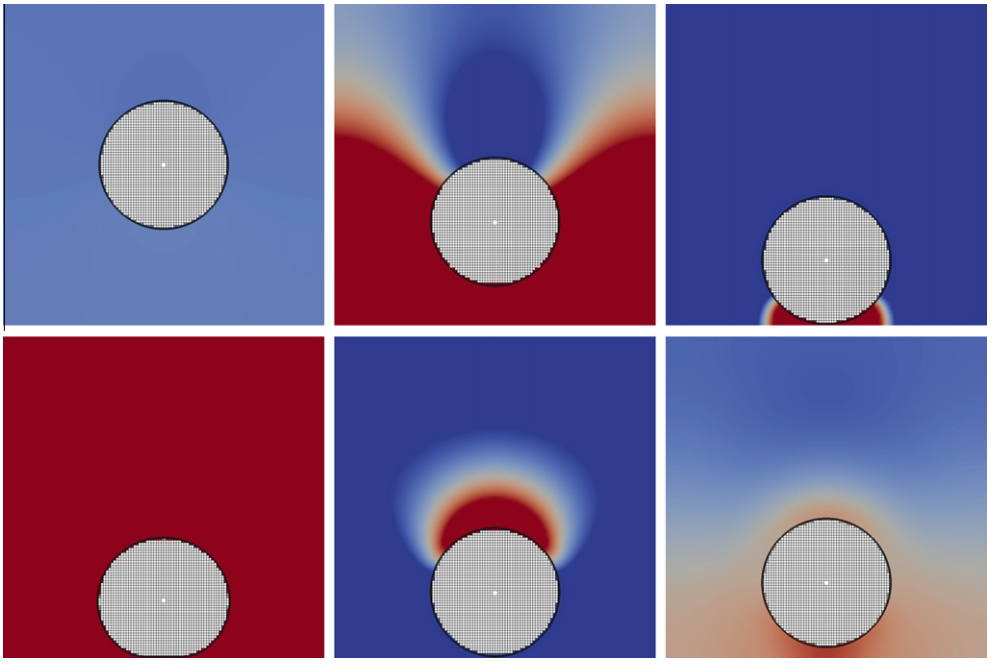

Fig. 7. Falling ball bouncing of the bottom wall. Snapshots of the solution at times $t = 0$, $t = 0.71$, $t = 0.96$ (first contact), $t = 1.035$ (biggest deformation), $t = 1.125$ (breaking contact) and $t = 1.38$ (highest bounce-off).

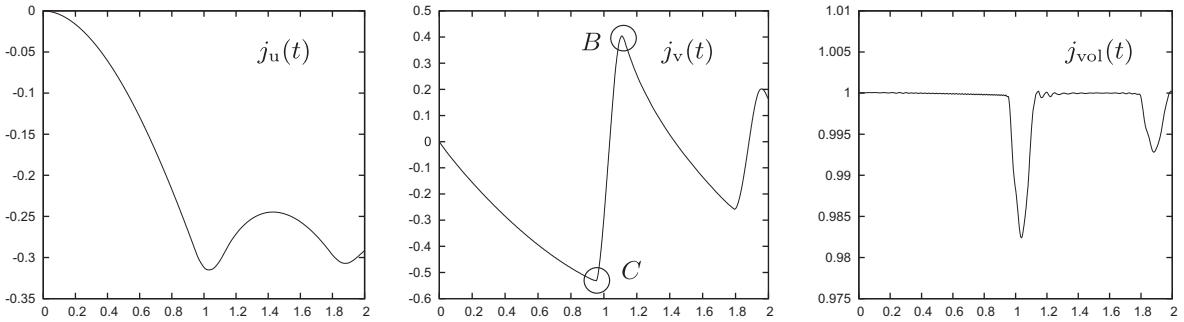

Fig. 8. Falling ball: functionals as plot over time. Left: solid's average deformation. Middle: solid's average velocity. Right: solid's relative volume. The two turning points of the velocity for contact (C) and maximum bounce-off (B) are indicated in the middle plot.

Table 3
Left: maximum (negative) velocity reached in free fall. Right: maximum average velocity after bounce-off. Calculations on three different spatial and temporal meshes.

h	k			k		
	0.0100	0.0050	0.0025	0.0100	0.0050	0.0025
2^{-5}	−0.4977	−0.4990	−0.5006	0.320	0.348	0.365
2^{-6}	−0.5248	−0.5286	−0.5298	0.318	0.369	0.396
2^{-7}	−0.5402	−0.5311	−0.5315	0.357	0.388	0.404

Table 4
Error in mass conservation for the falling ball.

h	k		
	0.0100	0.0050	0.0025
2^{-5}	$2.68 \cdot 10^{-3}$	$2.66 \cdot 10^{-3}$	$2.69 \cdot 10^{-3}$
2^{-6}	$7.82 \cdot 10^{-4}$	$6.95 \cdot 10^{-4}$	$6.72 \cdot 10^{-4}$
2^{-7}	$2.63 \cdot 10^{-4}$	$1.92 \cdot 10^{-4}$	$1.68 \cdot 10^{-4}$

In Table 3 we indicate the maximum (negative) velocity that is reached at the time of first contact $t_C \approx 0.952$, as well as the maximum velocity that is reached after the first bounce-off $t_B \approx 1.105$, see Fig. 8. Computations are done using three different temporal and spatial discretization parameters h and k. All meshes are uniform in space and time. While the time-step has only a very small influence on the functional values we observe convergence under mesh-refinement.

Finally, in Table 4 we give the temporal error with regard to mass conservation

$$\|j_{\text{mass}}(t) - \hat{\rho}_s \pi r_{\text{ball}}^2\|_{L^2([0,2])}, \quad j_{\text{mass}}(t) := \int_{\Omega_s(t)} J_s \hat{\rho}_s \, \mathrm{d}x.$$

Here, we observe $O(h^2)$ convergence. Being an interface-capturing method like Level-Sets, this result has to be expected for linear finite elements. The time-discretization parameter k appears to be too small to have a substantial influence on the accuracy. The question of mass conservation is of great importance in the context of this Eulerian formulation, since the method by construction does not strictly guarantee this conservation.

6. Outlook

In this paper we investigate a new, fully Eulerian variational formulation for fluid–structure interaction problems. The fully Eulerian formulation allows us to treat FSI problems with freely moving structures and with large deformations. This is the main advantage of the Eulerian method compared to interface tracking methods such as the arbitrary Lagrangian–Eulerian (ALE) method.

The method based on the Eulerian approach is inherently more expensive than the ALE method, since a careful capturing and discretization of the moving interface is necessary. Further, without local mesh adaptation at the interface, loss of accuracy and reduction to first order convergence has to be expected. One benefit of the Eulerian method is the standard description of the flow problem in Eulerian coordinates without the need to introduce additional variables and without the introduction of nonlinearities by means of domain transformations.

The Eulerian formulation allows the straightforward realization of problems with very large deformation, movement and even contact of the structure. Without the artificial domain mapping used in ALE approaches, the variational formulation is well-posed, even in the event of "near contact" where the elastic structure enters the last layer of mesh elements close to the boundary. This potential has been investigated for two model configurations.

In future work it will be of upmost importance to extend the discretization to a higher order scheme both in space and time. Here it will be necessary to use a fully implicit time-stepping scheme taking the domain movement into account. For this purpose it will be necessary to include shape derivatives with respect to the moving interface. Further, in the context of more realistic and three dimensional application problems an efficient multigrid solver for this monolithic coupled fsi-formulation must be developed. Both issues are subject to ongoing work.

References

[1] I. Babuška, A.D. Miller, The post-processing approach in the finite element method. I. Calculations of displacements, stresses and other higher derivatives of the displacements, Int. J. Numer. Methods Eng. 20 (1984) 1085–1109.
[2] Y. Bazilevs, V.M. Calo, T.J. R Hughes, Y. Zhang, Isogeometric fluid–structure interaction: theory, algorithms, and computations, Comput. Mech. 43 (2008) 3–37.
[3] R. Becker, R. Rannacher, An optimal control approach to a posteriori error estimation in finite element methods, in: A. Iserles (Ed.), Acta Numerica, vol. 37, Cambridge University Press, 2001, pp. 1–225.
[4] T. Belytschko, Fluid–structure interaction, Comput. Struct. 12 (1980) 459–469.
[5] M. Besier, W. Wollner, On the pressure approximation in nonstationary incompressible flow simulations on dynamically varying spatial meshes, Int. J. Numer. Math. Fluids 69 (2012) 1054–1064.
[6] M. Braack, G. Lube, Finite elements with local projection stabilization for incompressible flow problems, J. Comput. Math. 27 (2009) 116–147.
[7] M. Braack, T. Richter, Solutions of 3D Navier–Stokes benchmark problems with adaptive finite elements, Comput. Fluids 35 (4) (2006) 372–392.
[8] A.N. Brooks, T.J.R. Hughes, Streamline upwind Petrov–Galerkin formulation for convection dominated flows with particular emphasis on the incompressible Navier–Stokes equations, Comput. Methods Appl. Mech. Eng. 32 (1982) 199–259.
[9] E.H. van Brummelen, K.G. van der Zee, R. de Borst, Space/time multigrid for a fluid–structure-interaction problem, Appl. Numer. Math. 58 (12) (2008) 1951–1971.
[10] G.F. Carey, S.S. Chow, M.K. Seager, Approximate boundary-flux calculations, Comput. Methods Appl. Mech. Eng. 50 (1985) 107–120.
[11] J. Chessa, P. Smolinski, T. Belytschko, The extended finite element method (XFEM) for solidication problems, Int. J. Numer. Methods Eng. 53 (2002) 1959–1977.
[12] P.G. Ciarlet, Finite Element Methods for Elliptic Problems, North-Holland, Amsterdam, 1978.
[13] D. Coutand, S. Shkoller, Motion of an elastic solid inside an incompressible viscous fluid, Arch. Ration. Mech. Anal. (2005) 25–102.
[14] T. Dunne, An Eulerian approach to fluid–structure interaction and goal-oriented mesh refinement, Int. J. Numer. Math. Fluids 51 (2006) 1017–1039.
[15] T. Dunne. Adaptive finite element approximation of fluid-structure interaction based on Eulerian and arbitrary Lagrangian–Eulerian variational formulations. Ph.D. thesis, University of Heidelberg, 2007, urn:nbn:de:bsz:16-opus-79448.
[16] T. Dunne, R. Rannacher, T. Richter, Numerical simulation of fluid–structure interaction based on monolithic variational formulations, in: G.P. Galdi, R. Rannacher (Eds.), Comtemporary Challenges in Mathematical Fluid Mechanics, World Scientific, Singapore, 2010.
[17] C.A. Felippa, K.C. Park, M.R. Ross, A classification of interface treatments for fsi, in: H.-J. Bungartz, M. Mehl, M. Schäfer (Eds.), Fluid Structure Interaction II, Lecture Notes in Computational Science and Engineering, vol. 73, Springer, 2010, pp. 27–52.
[18] G.P. Galdi, R. Rannacher, A.M. Robertson, S. Turek (Eds.), Hemodynamical Flows: Modeling, Analysis and Simulation, Springer, Berlin, 2008.
[19] M.W. Gee, U. Küttler, W.A. Wall, Truly monolithic algebraic multigrid for fluid-structure interaction, Int. J. Numer. Meth. Engrg. 85 (2010) 987–1016.
[20] A. Gerstenberger, W.A. Wall, An extended finite element method/Lagrange multiplier based approach for fluid-structure interaction, Comput. Methods Appl. Mech. Eng. 197 (2008) 1699–1714.
[21] O. Ghattas, X. Li, A variational finite element method for stationary nonlinear fluid–solid interaction, J. Comput. Phys. 121 (1995) 347–356.
[22] R. Glowinski, T.W. Pan, T.I. Hesla, D.D. Joseph, J. Périaux, A fictitious domain approach to the direct numerical simulation of incompressible viscous flow past moving rigid bodies: application to particulate flow, J. Comput. Phys. 169 (2001) 363–426.
[23] P. He, R. Qiao, A full-Eulerian solid level set method for simulation of fluid structure interactions, Microfluid. Nanofluid. 11 (2011) 557–567.
[24] M. Heil, An efficient solver for the fully coupled solution of large-displacement fluid–structure interaction problems, Comput. Methods Appl. Mech. Eng. 193 (2004) 1–23.
[25] B.T. Helenbrook, Mesh deformation using the biharmonic operator, Int. J. Numer. Methods Eng. (2001) 1–30.
[26] J. Heywood, R. Rannacher, Finite element approximation of the nonstationary Navier–Stokes problem. iii. Smoothing property and higher order error estimates for spatial discretization, SIAM J. Numer. Anal. 25 (3) (1988) 489–512.
[27] J. Heywood, R. Rannacher, Finite element approximation of the nonstationary Navier–Stokes problem. iv. Error analysis for second-order time discretization, SIAM J. Numer. Anal. 27 (3) (1990) 353–384.
[28] J.G. Heywood, R. Rannacher, S. Turek, Artificial boundaries and flux and pressure conditions for the incompressible Navier–Stokes equations, Int. J. Numer. Math. Fluids 22 (1992) 325–352.
[29] C.W. Hirt, A.A. Amsden, J.L. Cook, An arbitrary Lagrangian–Eulerian computing method for all flow speeds, J. Comput. Phys. 14 (1974) 227–469.
[30] C.W. Hirt, B.D. Nichols, Volume of fluid (VOF) method for the dynamics of free boundaries, J. Comput. Phys. 39 (1981) 201–225.
[31] G.A. Holzapfel, Nonlinear Solid Mechanics: A Continuum Approach for Engineering, Wiley, Blackwell, 2000.
[32] J. Hron, S. Turek, A monolithic fem/multigrid solver for an ALE formulation of fluid–structure interaction with applications in biomechanics, in: H.-J. Bungartz, M. Schäfer (Eds.), Fluid–Structure Interaction: Modeling, Simulation, Optimization, Lecture Notes in Computational Science and Engineering, Springer, 2006, pp. 146–170.
[33] J. Hron, S. Turek, Proposal for numerical benchmarking of fluid–structure interaction between an elastic object and laminar incompressible flow, in: H.-J. Bungartz, M. Schäfer (Eds.), Fluid–Structure Interaction: Modeling, Simulation, Optimization, Lecture Notes in Computational Science and Engineering, Springer, 2006, pp. 371–385.
[34] J. Hron, S. Turek, M. Madlik, M. Razzaq, H. Wobker, J.F. Acker, Numerical simulation and benchmarking of a monolithic multigrid solver for fluid–structure interaction problems with application to hemodynamics, in: H.-J. Bungartz, M. Schäfer (Eds.), Fluid–Structure Interaction II: Modeling, Simulation, Optimization, Lecture Notes in Computational Science and Engineering, Springer, 2010, pp. 197–220.
[35] T.J.R. Hughes, W.K. Liu, T.K. Zimmermann, Lagrangian–Eulerian finite element formulations for incompressible viscous flows, Comput. Methods Appl. Mech. Eng. 29 (1981) 329–349.
[36] A.A. Johnson, T.E. Tezduyar, Mesh update strategies in parallel finite element computations of flow problems with moving boundaries and interfaces, Comput. Methods Appl. Mech. Eng. 119 (1994) 73–94.
[37] C. Johnson, Numerical Solution of Partial Differential Equations by the Finite Element Method, Cambridge University Press, Cambridge, UK, 1987.
[38] A. Legay, J. Chessa, T. Belytschko, An Eulerian–Lagrangian method for fluid–structure interaction based on level sets, Comput. Methods Appl. Mech. Eng. 195 (2006) 2070–2087.

[39] R. Leveque, Z. Li, The immersed interface method for elliptic equations with discontinuous coefficients and sinuglar sources, SIAM J. Numer. Anal. 31 (1994) 1019–1044.
[40] M. Luskin, R. Rannacher, On the smoothing property of the Crank–Nicholson scheme, Appl. Anal. 14 (1982) 117–135.
[41] S. Okazawa, K. Kashiyama, Y. Kaneko, Eulerian formulation using stabilized finite element methods for large deformation solid dynamics, Int. J. Numer. Math. Fluids 72 (2007) 1544–1559.
[42] S. Osher, R. Fedkiw, Level set methods and dynamic implicit surfaces, Appl. Math. Sci., Springer, 2003.
[43] C.S. Peskin, The immersed boundary method, Acta Numer. 11 (2002) 479–517.
[44] R. Rannacher, T. Richter, An adaptive finite element method for fluid–structure interaction problems based on a fully Eulerian formulation, in: H.J. Bungartz, M. Mehl, M. Schäfer (Eds.), Fluid–Structure Interaction II, Modelling, Simulation, Optimization, Lecture Notes in Computational Science and Engineering, vol. 73, Springer, 2010, pp. 159–192.
[45] T. Richter, Goal oriented error estimation for fluid–structure interaction problems, Comput. Methods Appl. Mech. Eng. 223–224 (2012) 28–42.
[46] T. Richter, T. Wick, Finite elements of fluid–structure interaction in ALE and fully Eulerian coordinates, Comput. Methods Appl. Mech. Eng. (2010), http://dx.doi.org/10.1016/j.cma.2010.04.016.
[47] J.A. Sethian, Level Set Methods and Fast Marching Methods Evolving Interfaces in Computational Geometry, Fluid Mechanics, Computer Vision, and Materials Science, Cambridge University Press, 1999.
[48] J. Sokołowski, J.-P. Zolésio, Introduction to Shape Optimization, Computational Mathematics, vol. 16, Springer, 1992.
[49] A.H. Stroud, Approximate Calculation of Multiple Integrals, Prentice-Hall, 1971.
[50] K. Sugiyama, S. Li, S. Takeuchi, S. Takagi, Y. Matsumoto, A full Eulerian finite difference approach for solving fluid–structure coupling problems, JCP 230 (2011) 596–627.
[51] K. Takizawa, T.E. Tezduya, Multiscale space–time fluid–structure interaction techniques, Comput. Mech. 48 (2011) 247–267.
[52] T.E. Tezduyar, Stabilized finite element formulations for incompressible flow computations, Adv. Appl. Mech. 28 (1992) 1–44.
[53] T.E. Tezduyar, S. Sathe, Modeling of fluid–structure interactions with the space-time finite elements: solution techniques, Int. J. Numer. Math. Fluids. 54 (2007) 855–900.
[54] P. van Hoogstraten, P.M.A. Slaats, F.P.T. Baaijens, A Eulerian approach to the finite element modelling of Neo-Hookean rubber material, Appl. Sci. Res. 48 (1991) 193–210.
[55] T. Wick, Fluid–structure interactions using different mesh motion techniques, Comput. Struct. 89 (2011) 1456–1467.
[56] T. Wick, Benchmark results for fluid–structure interaction problems in ale coordinates using different mesh motion techniques, Technical report, University of Heidelberg, 2012.
[57] K.G. van der Zee, E.H. van Brummelen, I. Akkerman, R. de Borst, Goal-oriented error estimation and adaptivity for fluid–structure interaction using exact linearized adjoint, Comput. Methods Appl. Mech. Eng. 200 (2011) 2738–2757.
[58] K.G. van der Zee, E.H. van Brummelen, R. de Borst, Goal-oriented error estimation and adaptivity for free-boundary problems: the shape-linearization approach, SIAM J. Sci. Comput. 32 (2) (2010) 1093–1118.